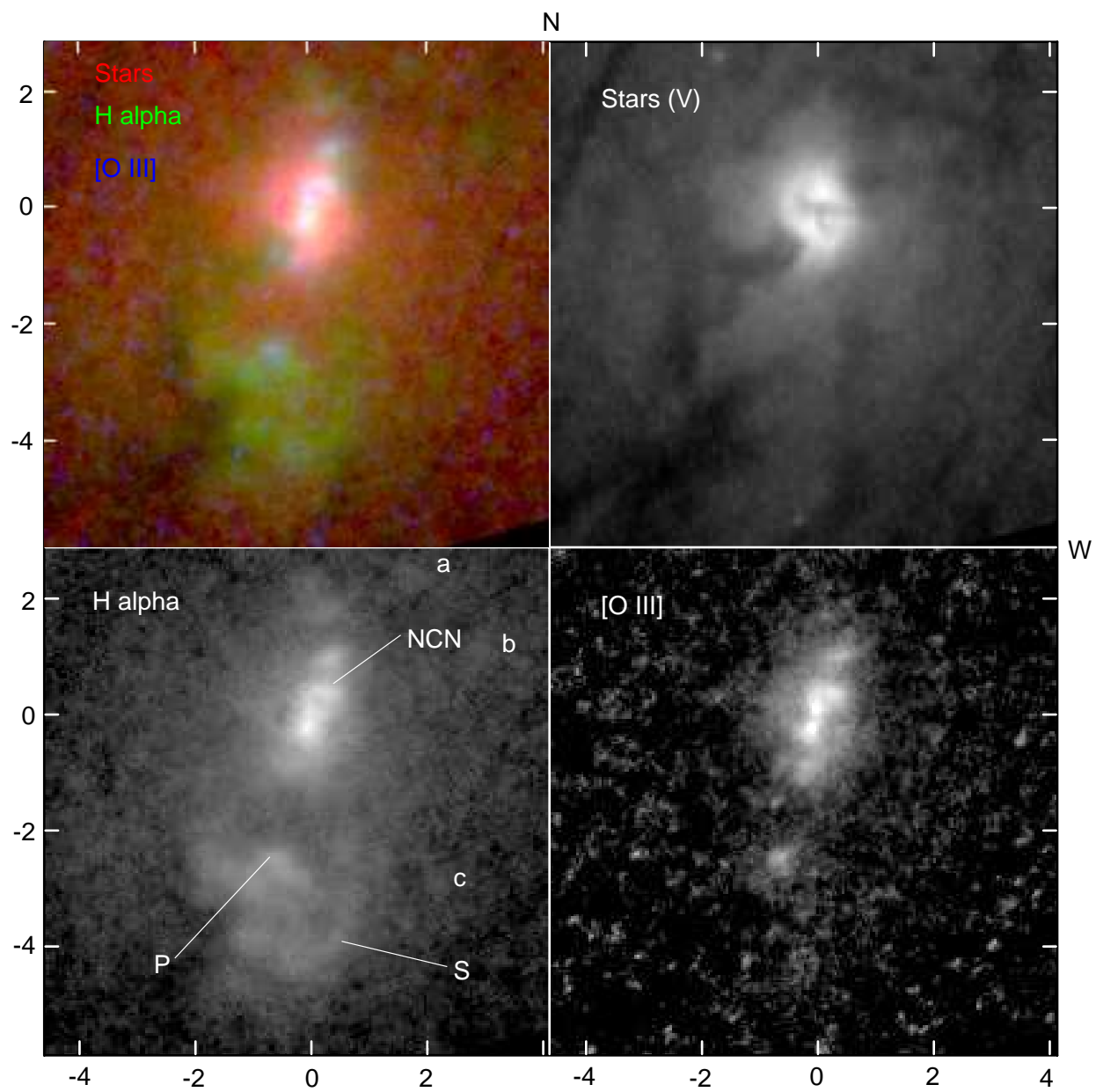


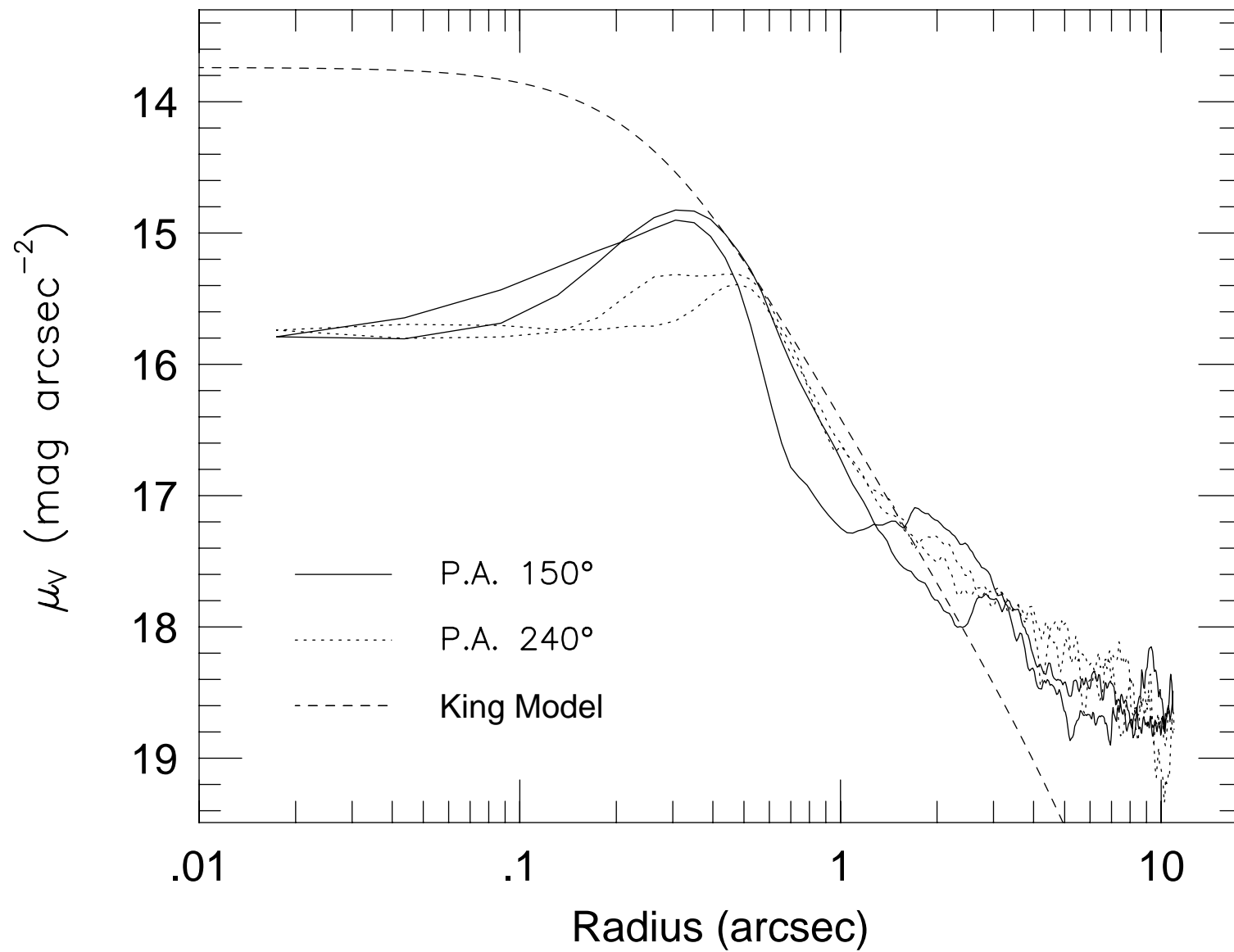
TABLE 1. Observing Log

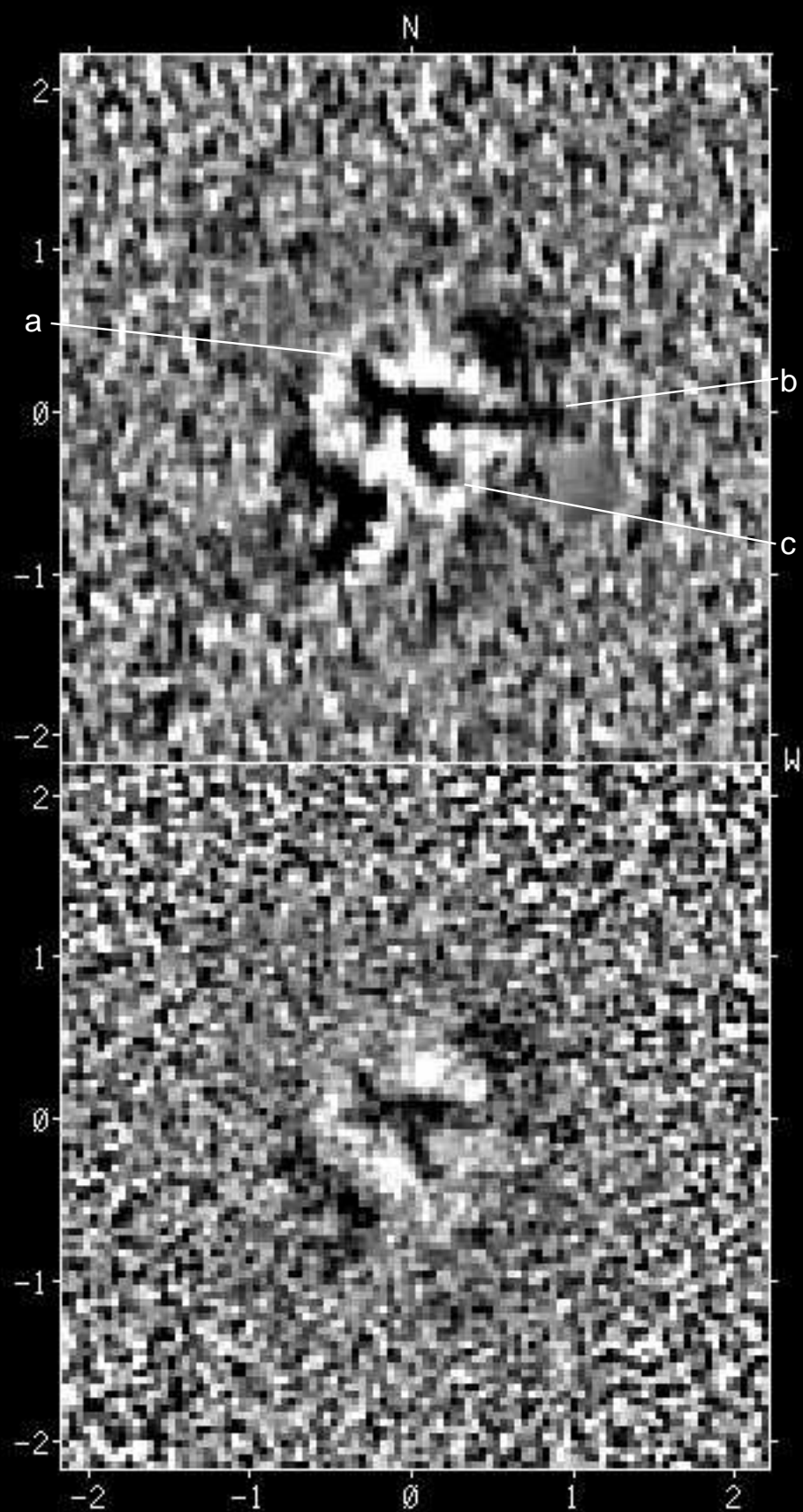
Target	Date	Filter	Exposure Time	V3 P.A. ^a
NGC 5194	Jul 14, 1992	F555W	100s	258.1°
NGC 5194	Jul 14, 1992	F555W	500s	258.1°
NGC 5194	Jul 14, 1992	F555W	500s	258.1°
NGC 5194	Dec 20, 1991	F547M	350s	123.7°
NGC 5194	Dec 20, 1991	F502N	1800s	123.7°
NGC 5194	Dec 20, 1991	F664N	900s	123.7°
NGC 5194	Dec 20, 1991	F664N	900s	123.7°

Notes to Table 1.

^aPosition angle, measured from N through E, of the V3 axis of the telescope.







This figure "m51fig5.gif" is available in "gif" format from:

<http://arxiv.org/ps/astro-ph/9610111v1>

The Nuclear Region of M51 Imaged with the *HST* Planetary Camera¹

Carl J. Grillmair

Jet Propulsion Laboratory, California Institute of Technology, 4800 Oak Grove Drive,
Pasadena, California 91109-8099

S. M. Faber

UCO/Lick Observatory, Board of Studies in Astronomy and Astrophysics, University of
California, Santa Cruz, California 95064

Tod R. Lauer

Kitt Peak National Observatory, National Optical Astronomy Observatories², P.O. Box
26732, Tucson, Arizona 85726

J. Jeff Hester

Department of Physics and Astronomy, Arizona State University, Tempe, Arizona
85287-1504

C. Roger Lynds

Kitt Peak National Observatory, National Optical Astronomy Observatories², P.O. Box
26732, Tucson, Arizona 85726

Earl J. O'Neil, Jr.

Kitt Peak National Observatory, National Optical Astronomy Observatories², P.O. Box
26732, Tucson, Arizona 85726

Paul A. Scowen

Department of Physics and Astronomy, Arizona State University, Tempe, Arizona
85287-1504

ABSTRACT

¹Based on observations with the NASA/ESA Hubble Space Telescope, obtained at the Space Telescope Science Institute, which is operated by AURA, Inc., under NASA contract NAS 5-26555.

²The National Optical Astronomy Observatories are operated by the Association of Universities for Research in Astronomy, Inc. (AURA) under cooperative agreement with the National Science Foundation.

We present high-resolution, broad- and narrow-band, pre-refurbishment images of the central region of M51 taken with the Planetary Camera of the *Hubble Space Telescope*. The *V*-band images show a rather chaotic distribution of dust lanes, though some are oriented radially, roughly aligned with the major axis of the bar, and may be transporting gas to the AGN in the nucleus. The dust lane obscuring the nucleus of the galaxy, which was previously thought to be an edge-on accretion disk feeding the AGN, is not centered on the nucleus. It is unlikely that this is a stable configuration, suggesting that the material has only recently entered the nuclear region. The nucleus is contained within a cluster of stars having a total luminosity of order $5 \times 10^7 L_{\odot}$. Fitting a King model to the least obscured portions of the cluster yields a maximum core radius of 14 pc. The morphology apparent in the forbidden-line images of the extra-nuclear cloud is consistent with a narrow jet striking and scattering off the boundary of a relatively dense cocoon of gas in the disk of the galaxy. The emission-line regions are concentrated along the inner borders of dust filaments, supporting the view that the nuclear jet is ramming into and stirring up the ISM of the disk.

Subject headings: galaxies: individual (NGC 5194) - galaxies: active - galaxies: Seyfert - galaxies: jets - galaxies: nuclei – galaxies: ISM

1. Introduction

M51 (NGC 5194, the “Whirlpool” galaxy) is a relatively nearby, nearly face-on, Sc spiral. Its proximity, combined with grand-design spiral arms and low-level nuclear activity have made it a popular target for both ground-based and space-based instrumentation. Goad, De Veny, & Goad (1979) first determined that M51 has a Seyfert-like nucleus, and Rose and Cecil (1983) measured line widths at zero intensity of $\sim 1800 \text{ km s}^{-1}$. Ford *et al.* (1985, hereafter FCJLH) showed that much of this activity originates outside the nucleus, specifically in a filled cloud to the south and a ring of emission-line regions to the north of the nucleus. Based on the high temperature of the gas in the cloud and the similarity of the emission-line ratios to those found in supernova remnants, they determined that the emission-line gas is probably excited by shocks rather than photoionization by a non-stellar source in the nucleus. The morphology and kinematics of the southern cloud led FCJLH to conclude that it was an expanding shell of gas in the disk of the galaxy, either inflated by a relativistic jet emanating from the nucleus, or ejected from the nucleus as a distinct plasmoid. These results were later confirmed and extended by Cecil (1988), who used imaging Fabry-Perot observations to map the narrow-line region and presented a detailed

model of a nuclear jet impinging on gas in the disk. Spencer & Burke (1972) discovered a weak, elongated nuclear radio source in M51, and Crane & van der Hulst (1992) used sub-arcsecond 6cm VLA observations to show that the extra-nuclear cloud and the nucleus are indeed connected by a narrow ($\leq 0.3''$) jetlike radio feature. However, the energy in the jet is less than that required to account for the total number of recombinations, and a non-thermal, nuclear source of ionizing radiation appears necessary.

Hubble Space Telescope (HST) images of the central regions of M51 were first taken in 1991, and these were briefly discussed by Kinney *et al.* (1992) and Mitton (1992). Most striking was the F547M image, which showed an “X”-shaped dust feature obscuring the nucleus. The main East-West bar of the “X” was roughly perpendicular to the radio jet, leading some to speculate that we were looking edge-on at a torus of material surrounding and presumably feeding the massive black hole assumed to be powering the jet.

As part of an ongoing GTO project to study the physical conditions in the nuclei of relatively nearby galaxies, we have acquired high-resolution, *V*-band Planetary Camera images of the central region of M51. We present and briefly discuss these images, along with complementary narrow-band images from the HST archive.

2. Observations.

Planetary Camera (PC) images of the nuclear region of M51 were taken in July of 1992 using filter F555W (roughly corresponding to the Johnson *V* band) as part of Wide Field/Planetary Camera (WF/PC I) Guaranteed Time Observer program 3639. Narrow-band images were taken in December of 1991 as part of Faint Object Spectrograph General Observer program 3194. All images were taken during the pre-refurbishment period, when the optics were affected by spherical aberration. Details concerning these images are given in Table 1. The PC constitutes the high resolution component ($0.044 \text{ arcsec pix}^{-1}$) of WF/PC I and is described in detail by Griffiths (1989). Assuming a distance to M51 of 9.6 Mpc (Sandage and Tammann 1974), one PC pixel corresponds to 2.0 pc. Guiding during all observations was carried out in coarse track, with the core of the galaxy approximately centered on chip PC6. Pointing during the F555W exposures was excellent, and the three frames were found to be coincident to within 0.1 pixels.

All images were reduced following the procedures outlined by Lauer (1989). For F555W and F664N, most cosmic rays events were removed by pixel-by-pixel comparison of image pairs, and the few remaining obvious cosmic rays were removed interactively. Only single images were available in F502N and F547M, and obvious cosmic rays were identified

interactively and removed by interpolation.

Deconvolution of WF/PC 1 images has become the standard procedure for extracting information on scales approaching the diffraction limit of the uncompromised telescope optics (*e.g.* Lauer *et al.* 1991). The F555W image was deconvolved with a composite Point-Spread-Function (PSF) constructed using several dedicated PSF exposures of stars taken during the period June through September 1992. The focus changes during this period were relatively minor (Hasan, Burrows, & Schroeder 1993), and the composite PSF has a signal-to-noise ratio considerably better than that of the individual images. Eighty iterations of the Lucy-Richardson deconvolution algorithm (Richardson 1972; Lucy 1974) were applied to the coadded F555W image, and the results are shown in Figure 1 (Plate 1).

For F547M and the narrow-band images, we used PSFs generated using Tiny Tim v2.1 (Krist 1992). While the fine structure in the observed PSF is not well modeled by any existing software, the gross characteristics and encircled-energy profiles shown by these models represent the PSFs quite well. Due to the smaller number of photons in these images, significant mottling of the deconvolved images became noticeable beyond 20 iterations, and deconvolution was halted at this point. Continuum levels in the narrow-band and F547M images were measured by determining the modes of the pixel intensity distributions in regions devoid of emission-line flux. The suitably-scaled F547M image was then subtracted from each of the narrow-band images. In Figure 2 we show the results for the central 9×9 arcseconds for F664N and F502N after 20 Lucy-Richardson iterations for the central regions of the galaxy. Also shown for comparison in Figure 2 is the central portion of the F555W image after 80 deconvolution iterations. Deconvolution was carried out on much larger (512×512 pixels) portions of the images, and the regions shown in Figure 2 are unaffected by edge effects.

The frames shown in Figure 2 and subsequent figures have been rotated according to the position angle of the V3 axis of the telescope at the time of observation (Table 1). The coordinates in all cases are with respect to a point lying midway between the two brightest features near the nucleus in the F555W image (see below). The spatial offsets between the F555W and F547M images were determined by centroiding 7 stars visible in both frames, yielding $\Delta x = 39.42 \pm 0.14$ and $\Delta y = 69.05 \pm 0.14$ pixels, where the uncertainties are errors in the mean. Due to the low signal-to-noise ratio, offsets between the F664N, F502N, and the F547M images (which were all taken at a single epoch) rely heavily on a single point-source situated $\approx 30''$ from the nucleus. However, several highly-structured regions in the field were also cross-correlated, and the resultant offsets were found to be in good agreement with the offsets determined using the point-source. In all cases, the offsets were found to be ≤ 1 pixel.

3. Discussion

3.1. Stars and Dust

Among the more striking features in Figure 1 are the many dust lanes in and around the nucleus of M51. Some of the dust lanes are oriented almost radially, and several filaments apparently penetrate the stellar concentration at the center, providing evidence of radial gas transport. The main radial flows appear to be directed roughly along the major axis of the bar and stellar oval (Pierce 1986). There is some suggestion that the major northern radial dust lane passes by the nucleus, then turns sharply to enter the nucleus from the south, similar to the flow patterns expected if the semimajor axis of the bar is much smaller than the Lagrangian radius (Athanasoula 1992). However, the overriding impression near the nucleus is one of chaos, with dust filaments oriented in all directions, often sinuous and intersecting with one another. This is interesting in that, in the absence of a stirring mechanism, a dissipative gaseous medium would be expected to settle into a pattern of smooth, non-intersecting flow lines. Yet there appear to be few bright (and therefore young) stars in this region to provide the energy required to disturb such a pattern. Indeed, comparing with the surface density of luminous stars at the perimeter of the oval at $\approx 7''$, star formation appears to be somewhat suppressed near the nucleus.

The nucleus is apparently embedded in a large, central cluster of stars and is itself obscured by narrow, intersecting dust lanes. That this central cluster is distinct from the disk is shown in Figure 3, where we have plotted surface brightness profiles along the major and minor axes of the bar. The profiles have been computed from 3-pixel-wide cuts across the image at position angles 150° and 240° , respectively. Though we cannot reliably decompose the cluster and disk components due to the complexity of the dust distribution, the cluster component evidently dominates the light profile within $\approx 1''$. The profile least affected by obscuration seems to be the western cut along the minor axis at P.A. 240° , which exhibits a power-law slope $\alpha \approx -1.7$ in the region $0.5'' < r < 1.5''$. For comparison, we show a King model (dashed line) having $r_c = 0.3''$ and a concentration parameter of 100. Constructing a 2-dimensional image of the King model shown in Figure 3 and varying the pixel location of the center, we obtain the best visual match to the observations using a centroid located midway along the line connecting the two brightest pixels on either side of the main nuclear dust lane. This point is used to define the origin for the coordinate system used in the plates.

The King model appears to be a reasonable approximation to the surface brightness profile of the cluster in the region least affected by disk stars or dust. The value of r_c may be much smaller than our best-eyeball-fit value without affecting the fit in the dust-free region, and $r_c = 0.3'' \pm 0.05''$ ($= 14$ pc) constitutes an upper limit. Since the nucleus is obscured, we

cannot measure the central stellar surface brightness. Even assuming that a King model is a valid representation for the distribution of stars in the core, the central surface brightness predicted in Figure 3 can be regarded as no more than a lower limit. Most of the unobscured galactic nuclei so far studied with the Planetary Camera show nuclear cusps of varying degrees of steepness (Lauer *et al.* 1995), and it is entirely possible that the underlying stellar distribution in the nucleus of M51 is also more highly concentrated than a King model. The total luminosity within $0.3''$ predicted by the King model is $2.3 \times 10^7 L_{\odot}$, and the corresponding central luminosity density is $4200 L_{\odot} \text{pc}^{-3}$. Assuming orbital isotropy and adopting a central velocity dispersion of 118 km s^{-1} (Whitmore, McElroy, & Tonry 1985), we obtain a formal value for the V -band core mass-to-light ratio of $2.8 M_{\odot}/L_{\odot}$. The actual value could be either higher or lower depending on the trend of the product (Ir) near the origin.

Previous reports discussing the F547M image have described the dust lanes obscuring the nucleus as having an “X” configuration. This morphology has variously been interpreted as an edge-on disk and a separate band of dust (Kinney *et al.* 1992) or possibly two intersecting disks viewed edge-on (Cowen 1992). This “X”-morphology is not nearly as evident in the F555W image, and the question arises whether this difference is due to the increase in signal-to-noise ratio or to contamination of the F555W image by line emission.

In Figure 4 we have subtracted the line-emission components from the F555W image and “unsharp-masked” the result to enhance the contrast on small scales. The F664N and F502N images were each scaled to the F555W exposure time, and scaled again using the relative system throughputs at the appropriate locations in the F555W band-pass as given in the WFPC Handbook. The sum of these two images was then subtracted from the F555W image, and the result was divided by a slightly smoothed version of itself. In the region where the $H\alpha$ /[NII] emission is most intense ($0''.17$ southwest of the nucleus), $H\alpha$ /[NII] and [OIII] emission contribute a relatively modest 2% and 4% of the total flux in the F555W image, respectively. To within the uncertainties, this agrees with a flux measurement made at the same position after scaling and subtracting the F547M image from the F555W image. We conclude that the apparent differences between the F555W and F547M images are primarily due to differences in signal-to-noise ratio and resolution. The F547M image, divided by a slightly smoothed version of itself, is shown in the lower panel of Figure 4 for comparison.

In the upper panel of Figure 4, the main, elongated, nuclear dust lane (MNDL) running east-west across the nucleus, while roughly centered in the transverse direction, does not appear to be centered on the nucleus along its length. The western end of the MNDL evidently extends at least $1''.1$ from the center of the central cluster, while the eastern end of the dust lane ends fairly abruptly at $\sim 0''.4$. If the MNDL were an edge-on, equilibrium,

circular disk, it would be orbiting a point at least 16 pc removed from the center of the central star cluster. This would not be a stable configuration, and we believe that the MNDL is more likely to be part of a tidally-sheared cloud of material that recently entered the nuclear region on a plunging orbit, the plane of which may be nearly coincident with our line of sight. The fact that the long axis of the MNDL is nearly perpendicular to the radio jet (see below) may simply be a consequence of the much shorter survival time of any dust filaments whose orbits would carry them into the path of the jet. Surprisingly, there appears to be no obvious connection between the MNDL and any of the larger, extra-nuclear dust filaments.

Closer inspection of the upper panel in Figure 4 reveals what appears to be substantial, westward “curling” of the secondary nuclear dust lane (the cross bar of the “X”) both to the north and to the south of the MNDL. This would be naturally consistent with a ring or disk of material approximately 52 pc in diameter, orbiting the nucleus, and oblique to both the radio jet and to our line of sight. The center of the partial ellipse traced by the dust falls within 2 pixels of the center of the central star cluster, and the missing northwestern portion of the ring might simply be hidden from view by the stars in the cluster. However, the line-subtracted F555W image (and to a lesser extent the F547 image) shows an apparent discontinuity between the northern and southern secondary dust lanes. There is some uncertainty in regard to the amount of continuum light at the juncture of the MNDL and the southern, secondary dust lane stemming from the use of different PSFs and levels of deconvolution in the F555W and narrow-band images. Nonetheless, no reasonable scaling of the narrow-band images can remove the apparent discontinuity, and we conclude that the northern and southern secondary dust lanes are probably physically distinct. Indeed, based purely on continuity arguments, it appears in Figure 4 that the northern secondary dust lane bends towards the south as it crosses the MNDL, giving rise to the $0''.2$ dust feature extending south from the eastern end of the MNDL.

3.2. Emission-Line Regions

In Figure 5 we compare the spatial distributions of $H\alpha$ and 6cm radio emission with one another, and with distributions of [OIII] and F555W flux. FCJLH first showed, based on optical and radio luminosity and on the forbidden-line widths, that the primary site of activity in M51 is an extra nuclear cloud (XNC) lying $\approx 3''$ south of the nucleus. Moreover, the emission-line ratios observed in the XNC were found to be similar to those in the shock-excited gas in some supernova remnants (SNRs), though the minimum energy computed for the XNC is roughly two orders of magnitude larger than that computed for the very radio-luminous Galactic SNR Cas A. Combining this with the limb-brightened morphology of the

XNC, the inferred mass motions, and the abrupt changes in the spectral characteristics going from the disk to the XNC, FCJLH concluded that the gas in the XNC is excited by shocks rather than photoionization by a central source. The scale of the phenomenon, along with the presence of a large ring of optical emission with similar spectral characteristics $9''$ northwest of the nucleus on a line joining the nucleus and the XNC, suggested that the ultimate source of the activity was in the nucleus. FCJLH proposed that a nuclear jet, creating shocks and inflating bubbles of gas in the disk, might be the source of the activity in the XNC.

Cecil (1988) used Fabry-Perot observations to investigate the kinematics of the gas in the nuclear regions of M51 and found, among other things, that the nucleus and the XNC were connected by a tongue of high-velocity, ionized gas. He also found that the largest range of gas velocities was to be found at the point labeled P in Figure 2. He largely confirmed and extended the work of FCJLH, developing a model in which a nuclear jet, directed into the plane of the disk (and making an angle of about 70° with our line of sight), strikes the periphery of a dense cocoon of material at an oblique angle (at P) and is scattered to form a secondary shock front (the arcuate feature labeled S in Figure 2). Crane & van der Hulst (1992) later found a very narrow, jet-like radio feature connecting the nucleus with P , strongly supporting the jet-hypothesis for the the origin of the bubbles. The naturally-weighted, 6cm VLA radio map of Crane & van der Hulst is shown superimposed on the F555W and F664N images in the upper panels of Figure 5.

Near the nucleus, the F664N image (Figure 2) reveals extended regions of relatively low-level emission, as well as localized areas of rather more intense activity. In Figure 5 we show contours of $H\alpha/[NII]$ emission (as measured from the F664N image) superimposed on F555W and F502N. The isopleths immediately surrounding the nucleus are significantly elongated, with the long axis pointed almost directly at P . The strongest emission is found $0''.2$ to the south of the MNDL in a narrow, $0''.2$ -long feature aimed about 10° eastwards of P . To the north of the MNDL, the strongest $H\alpha/[NII]$ emission ($\approx 25\%$ less intense than the peak emission to the south of the MNDL) is located just on the edge of the MNDL, within $0''.1$ of the center of the central star cluster. It is perhaps noteworthy that this northern source does not lie on the line projected along the long axis of the southern feature (the northern source is situated about $0''.15$ too far to the east). On the other hand, a line connecting the northern and southern emission peaks projects to lie almost on top of P . The apparent morphologies of the emission peaks may be largely a consequence of variable extinction in the vicinity of the MNDL. Alternatively, this may also be evidence for the presence of optical “wobbles” in the jet of the sort seen in other active nuclei. The line connecting P with the nuclear emission peaks makes an angle of $79^\circ \pm 2^\circ$ with the long axis of the MNDL.

The regions of peak nuclear emission in F502N correspond almost exactly with the loca-

tions of peak emission in F664N. However, the two F502N peaks on either side of the MN DL have very similar peak intensities, and both peaks are relatively compact, with FWHM $\sim 0''.17$. The pattern of nuclear [OIII] emission appears roughly biconical (with opening angle $\approx 45^\circ$), consistent with the presence of twin ionization cones along the path of the jet. Just as in the case of F664N, the apparent centerline of the southern ionization cone differs by about 10 degrees from the radial passing through P , though the northern and southern peaks together point almost directly at P .

Using an aperture of radius $0''.1$ and the system throughput curves given in the WFPC Handbook, we find for the southern peak $F(\text{H}\alpha + [\text{NII}]) = 2.5 \times 10^{-14} \text{ ergs s}^{-1} \text{ cm}^{-2}$ and $F([\text{OIII}]) = 9.5 \times 10^{-15} \text{ ergs s}^{-1} \text{ cm}^{-2}$. For the northern peak, we find $F(\text{H}\alpha + [\text{NII}]) = 1.9 \times 10^{-14} \text{ ergs s}^{-1} \text{ cm}^{-2}$ and $F([\text{OIII}]) = 9.3 \times 10^{-15} \text{ ergs s}^{-1} \text{ cm}^{-2}$. The uncertainties due to photon statistics are $\approx 1 \times 10^{-16} \text{ ergs s}^{-1} \text{ cm}^{-2}$ in each case. The emission at the nucleus itself is about a factor of two less than the emission from the peaks on either side. If the depression is due to absorption by the MN DL and the extinction in the V-band is approximately 2 magnitudes (assuming that the King model in Figure 3 gives a reasonable indication of the underlying stellar central surface brightness), this would be roughly consistent with the extinction properties of dust in our own Galaxy.

$0''.5$ north of the northern emission peak, visible in both F664N and F502N, is the Northern Compact Nebula (NCN) first described by Goad & Gallagher (1985). The region measures about $0''.5 \times 0''.2$ and its long axis is roughly perpendicular to the direction of the radio jet. Two similarly-shaped, though somewhat fainter regions are evident $1''.0$ and $1''.8$ north of the nucleus, respectively. The 6cm radio contours suggest enhanced radio emission in these regions as well. Goad & Gallagher found that the radial velocities measured in the NCN were about 35 km s^{-1} greater than predicted using the rotation curve of Goad, De Veny, & Goad (1979), and that the [NII] line widths were $\text{FWZI} \geq 300 \text{ km s}^{-1}$. Examining both F555W and Figure 4, we find patches or filaments of dust adjacent to and radially outwards from each of the three regions of $\text{H}\alpha/[\text{NII}]$ emission. The NCN itself may also be an extension of the northern secondary dust lane discussed previously. FCJLH put forth a ring of $\text{H}\alpha/[\text{NII}]$ emission $9''$ north of the nucleus as evidence for a now-extinguished, northwards-directed, nuclear jet. The high velocity widths in the NCN, combined with the extended radio emission to the north, suggest that a residual jet or wind in this region continues to interact with the ISM in the disk.

Beyond $1''$ from the nucleus, the strongest source of $\text{H}\alpha/[\text{NII}]$ and [OIII] emission is at P , consistent with Cecil's contention that P corresponds to the primary contact between the nuclear jet and a relatively dense cloud of gas in the disk. Inspection of Figure 5 reveals that P is indeed situated at the inner end of a large, radially-oriented, dust filament. P is resolved

in both F502N and F664N, and visibly elongated perpendicular to the direction of the jet. The peak [OIII] emission in the extra-nuclear cloud is coincident (to within ~ 1 pixel) of the peak emission in $H\alpha$ /[NII]. The integrated [OIII] flux within $0''.3$ of the brightest pixel in P is 8.6×10^{-15} ergs s $^{-1}$ cm $^{-2}$, of which half falls in an aperture of radius $0''.17$ (8 pc). This is consistent with the diameter of the radio jet ($0''.3$) estimated by Crane & van der Hulst (1992). While it is possible that the apparent size of P may be in large part due to the distribution of gas in the disk, the similarity in cross section between P and the radio feature would be consistent with a jet which remains highly collimated, despite its somewhat sinuous appearance in the radio map.

The arcuate emission region southwest of P (Cecil’s structure S) borders for some of its length a dusty arc of similar proportions. A cut across the shock front at its narrowest point (very near the end of the pointer indicating structure S in Figure 2) yields a FWHM $\approx 0''.3$, making it only barely resolved. The morphology of S is consistent with the inflation model of Cecil (1988), though the features we see probably tell us more about the distribution of gas in the disk than about the mechanics of the shock front.

There is a good spatial correlation (best revealed by blinking images) between the F664N-bright regions and the radial dusty regions visible in F555W extending along either side of the radio jet. The emission is distributed primarily along the inner edge of the dust, extending from the nuclear region to well past P . This implies significant interaction between the jet and the disk material along the whole length of the jet, and not just at P and S . Could the jet itself, by interacting with the gas in the disk, be responsible for the chaotic appearance of the dust filaments in Figure 1? FCJLH measured a total optical luminosity in the XNC of 3.6×10^{41} ergs s $^{-1}$. Assuming that the jet has been injecting this amount of energy into the disk over the past 10^7 years (equivalent to one orbital period at $10''$), we obtain a total energy input of 2×10^{56} ergs. This may be compared with the total orbital energy within $10''$ of the nucleus of 6×10^{56} ergs, computed by integrating over the surface brightness profile in Figure 2 and using $v_{rot} = 14.53R$ for $R < 9''$ (Goad, De Veny, & Goad 1979). Since the gas accounts for only a fraction of the total mass in this region, there is clearly more than sufficient energy in the jet to substantially stir up the ISM. Radiative dissipation would tend to smooth out any jet-induced turbulence on timescales of an orbit or two, and the appearance of the dust in the Figure 1 suggests that the stirring of the ISM by the jet has been either ongoing or recurrent for at least the last 10^7 years.

Outside the nucleus, the NCN, and the XNC, we see relatively low signal-to-noise ratio $H\alpha$ /[NII] enhancements, three of which are labeled a , b , and c in Figure 2. In all cases, the emitting regions seen in F664N correspond to regions of at least some obscuration in F555W. Region a appears in F555W to be an apparently isolated patch of dust, while b and c are

situated very near the apparent intersections of two dust filaments. The former is perhaps being illuminated by leakage of ionizing radiation from the central source, while the latter, if the intersections of the dust filaments are not merely chance projections, may result from the shock-induced heating of physical collisions between filaments.

In the upper panels of Figure 5 we compare the 6cm VLA radio observations (as digitized from Crane & van der Hulst 1992) with the F664N image. The radio contours have been shifted $0''.2$ west and $0''.6$ north to bring the region of peak radio emission into agreement with the optical position of the nucleus. The disagreement between the VLA and *HST* coordinates is within local astrometric uncertainties (Evans *et al.* 1991). After shifting, there is good, detailed agreement between the contours of the 6cm emission and the regions of ionization in the XNC. The radio emission shows a relatively steep gradient in the vicinity of the emission-line arcs, with the peak radio flux concentrated *within* structure *S*. This is consistent with the identification of *S* with the high-temperature bow shock of an expanding shell. On the other hand, it appears that the optical hot spot is not a feature in the radio emission. This would suggest that the radio emission comes from particles from the nucleus, rather than from particles accelerated in the post shock flow. It also suggests that these particles are not escaping upstream of the shock, because if they could get into the strong magnetic fields behind the radiative shocks, we would see a strong brightening in the radio flux just outwards of the bow shock.

The radio contours are compared with the F555W image in Figure 5. Given the correspondence between the radio contours and the $H\alpha/[NII]$ emission, and the tendency for the $H\alpha/[NII]$ emission to lie along the inner borders of some of the dust filaments, we expect that the radio contours might also be correlated with regions of dust obscuration. The radio contours do indeed trace the outlines of some of the dust features south of the nucleus, supporting the view that the bubble is interacting with the dust.

4. Summary

Broad and narrow-band Planetary Camera imaging of the nuclear region of M51 has added support to currently-held views concerning the source of the nuclear activity, and has raised new questions concerning the fueling of the mini-AGN at the center. In particular, we conclude

- (i) that the distribution of small-scale dust filaments within $7''$ of the nucleus appears largely chaotic,
- (ii) that the dust lane obscuring the center of M51 is extended too far in one direction to

be part of a stable torus of material orbiting the AGN,

- (iii) that the center of M51 is dominated by an apparently discrete cluster of stars which is an order of magnitude more luminous than the brightest Galactic globular cluster,
- (iv) that the width of the [OIII] emission region in the extra-nuclear cloud is consistent with the radio observations, which suggest a jet which is of order 10 pc or less in diameter, and
- (v) that the emission-line regions are generally confined to the inner boundaries of dust filaments, supporting the view that the jet is ramming through (and stirring up) the ISM in the disk.

Multi-color and narrow-band observations with the refurbished *HST* will allow a more complete study of the structure of the nucleus of M51 and the properties of the gas and dust. Near IR observations would be particularly useful to minimize the obscuring effects of the dust and allow us to more closely examine the region immediately surrounding the AGN. High-resolution, HST spectrophotometry will be needed to establish densities, temperatures, chemical compositions, and ionization mechanisms in the nuclear environs.

We are grateful to Bill Mathews for useful discussions during the analysis of these images. This research was conducted by the WF/PC Investigation Definition Team, supported in part by NASA Grant No. NAS5-1661.

REFERENCES

- Athanassoula, E. 1992, MNRAS, 259, 345
- Cecil, G. 1988, ApJ, 329, 38
- Crane, P. C., & van der Hulst, J.M. 1992, AJ, 103, 1146
- Cowen, R. 1992, *Science News*, 141, 390
- Evans, I. N., Ford, H. C., Kinney, A. L., Antonucci, R. J., Armus, L., & Caganoff, S. 1991, ApJ, 369, L27
- Ford, H. C., Crane, P. C., Jacoby, G. H., Lawrie, D. G., & van der Hulst, J. M. 1985, ApJ, 293, 132
- Goad, J. W., De Veny, J. B., & Goad, L. E. 1979, ApJS, 39, 439
- Goad, J. W., & Gallagher, J. S. 1985, ApJ, 279, 98
- Griffiths, R. 1989, *Wide Field and Planetary Camera Handbook*, (STScI publication, Baltimore)
- Hasan, H., Burrows, C. J., & Schroeder, D. J. 1993, PASP, 105, 1184
- Kinney, A. L., Kriss, G. A., Ford, H. C., Evans, I. N., Uomoto, A., Caganoff, S., & Tsvetanov, Z. 1992, *Bull. American Astron. Soc.*, 24, 727
- Krist, J. 1992, *The Tiny Tim User's Manual*.
- Lauer, T. R. 1989, PASP, 101, 445
- Lauer, T. R., Faber, S. M., Holtzman, J. A., Baum, W. A., Currie, D. G., Ewald, S. P., Groth, E. J., Hester, J. J., Kelsall, T, Kristian, J., Light, R. M., Lynds, C. R., O'Neil, E. J. Jr., Shaya, E. J., & Westphal, J. A. 1991, ApJ, 369, L41
- Lauer, T. R., Ajhar, E. A., Byun, Y. I., Dressler, A., Faber, S. M., Grillmair, C. J., Kormendy, J., Richstone, D., & Tremaine, S. 1995, AJ, 110, 2622
- Lucy, L. B. 1974, AJ, 79, 745
- Mitton, S. 1992, *New Scientist*, 1825, 15
- Pierce, M.J. 1986, AJ, 92, 285
- Richardson, W. H. 1972, *J. Opt. Soc. A.*, 62, 52
- Rose, J.A., & Cecil, G. 1983, ApJ, 266, 531
- Sandage, A.R., & Tammann, G.A. 1974, ApJ, 194, 559
- Spencer, J.H., & Burke, B.F. 1972, ApJ, 176, L101

Whitmore, B.C., McElroy, D.B., & Tonry, J.L. 1985, ApJS, 59, 1

Fig. 1.— F555W Planetary Camera image of the core region of M51 after 80 iterations of the Lucy-Richardson deconvolution algorithm. The stretch is logarithmic, and the coordinates are seconds of arc with respect to the assumed position of the nucleus (see text).

Fig. 2.— Broad-band and continuum-subtracted narrow-band images of the nuclear region of M51. The stretch in all cases is logarithmic, and the images have been rotated so that North is up and East is to the left. The F555W (V) image has undergone 80 Lucy-Richardson deconvolution iterations, while deconvolution of the lower signal-to-noise ratio narrow-band images was halted at 20 iterations. The upper left panel shows a combination of the images in the three other panels, with the color associations as indicated. The primary (P) and secondary (S) contacts between the nuclear flow and the disk material (see text) are indicated in the lower-left panel, as is the Northern Compact Nebula (NCN). Local $H\alpha$ enhancements which appear to be related to features visible in F555W are situated at a , b , and c .

Fig. 3.— V -band surface brightness profiles along the major and minor axes of the central bar. The dashed line is a King model with core radius $r_c = 0''.3$ and tidal radius $r_t = 30''$.

Fig. 4.— Unsharp-masked images of the central dust lanes in M51. For F555W (upper panel), the image shown in the upper-right panel of Figure 2 has been emission-line subtracted using the F664N and F502N images. For both F555W and F547M (lower panel), the images have been divided by median-window-smoothed versions of themselves to bring out the extended structure of the nuclear dust lanes. The stretch in both panels extends from 0.95 to 1.05. In the upper panel, the $0''.5 \times 0''.5$ region just south of the western end of the main nuclear dust lane is the result of an imperfectly removed flat-field defect. Indicated are features discussed in the text, including (a) the northern secondary dust lane, (b) the main nuclear dust lane (MNDL), and (c) the southern secondary dust lane.

Fig. 5.— F555W and continuum-subtracted, narrow-band images with superimposed 6cm and $H\alpha/[NII]$ contours. The contours in the upper two panels are the naturally-weighted, 6cm VLA observations of Crane & van der Hulst (1992). The contours in the lower panels derive from a slightly smoothed version of the continuum-subtracted F664N image.